

Cosmic Sign-Reversal: Non-Parametric Reconstruction of Interacting Dark Energy with DESI DR2

Yun-He Li¹ and Xin Zhang^{1, 2, 3, *}

¹*Liaoning Key Laboratory of Cosmology and Astrophysics,*

College of Sciences, Northeastern University, Shenyang 110819, China

²*MOE Key Laboratory of Data Analytics and Optimization for Smart Industry,*

Northeastern University, Shenyang 110819, China

³*National Frontiers Science Center for Industrial Intelligence and Systems Optimization,*
Northeastern University, Shenyang 110819, China

A direct interaction between dark energy and dark matter provides a natural and important extension to the standard Λ CDM cosmology. We perform a non-parametric reconstruction of the vacuum energy ($w = -1$) interacting with cold dark matter using the cosmological data from DESI DR2, Planck CMB, and three SNIa samples (PP, DESY5, and Union3). By discretizing the coupling function $\beta(z)$ into 20 redshift bins and assuming a Gaussian smoothness prior, we reconstruct $\beta(z)$ without assuming any specific parameterization. The mean reconstructed $\beta(z)$ changes sign during cosmic evolution, indicating an energy transfer from cold dark matter to dark energy at early times and a reverse flow at late times. At high redshifts, $\beta(z)$ shows a $\sim 2\sigma$ deviation from Λ CDM. At low redshifts, the results depend on the SNIa sample: CMB+DESI and CMB+DESI+PP yield $\beta(z)$ consistent with zero within 2σ , while CMB+DESI+DESY5 and CMB+DESI+Union3 prefer negative β at $\sim 2\sigma$. Both χ^2 tests and Bayesian analyses favor the $\beta(z)$ model, with CMB+DESI DR2+DESY5 showing the most significant support through the largest improvement in goodness of fit ($\Delta\chi^2_{\text{MAP}} = -17.76$) and strongest Bayesian evidence ($\ln \mathcal{B} = 5.98 \pm 0.69$). Principal component analysis reveals that the data effectively constrain three additional degrees of freedom in the $\beta(z)$ model, accounting for most of the improvement in goodness of fit. Our results demonstrate that the dynamical dark energy preference in current data can be equally well explained by such a sign-reversal interacting dark energy, highlighting the need for future observations to break this degeneracy.

I. INTRODUCTION

Recent measurements of baryon acoustic oscillations (BAO) from the Dark Energy Spectroscopic Instrument (DESI)[1, 2], when combined with cosmic microwave background (CMB) and type Ia supernovae (SNIa) data, suggest a hint of new physics in the nature of dark energy. The DESI Data Release 1 (DR1) results favor a time-varying equation of state (EoS) of dark energy at a significance of approximately 2.5σ to 3.9σ , depending on the SNIa dataset used [3]. This preference strengthens to 2.8σ to 4.2σ in the DESI DR2 analysis [4], presenting a notable challenge to the standard Λ CDM paradigm where dark energy is described by a cosmological constant Λ with a fixed EoS of $w = -1$. The DESI data have been widely used in recent cosmological analyses; see, e.g., Refs. [5–29].

While Λ CDM remains highly successful in fitting CMB data and explaining cosmic acceleration, it faces growing tensions with precision observations. A key discrepancy lies in the Hubble constant H_0 : local distance ladder measurements yield $H_0 = 73.04 \pm 1.04$ km/s/Mpc [30], whereas Λ CDM-based CMB analyses infer $H_0 = 67.36 \pm 0.54$ km/s/Mpc [31], revealing a tension exceeding 5σ . Theoretically, the cosmological constant faces

long-standing fine-tuning and coincidence problems [32–40]. This situation motivates modifications to the Λ CDM framework, such as replacing the cosmological constant with dynamical dark energy (with an EoS not exactly equal to -1), or adopting modified gravity theories that avoid introducing dark energy (see Ref. [41] for a recent review).

Cosmological models, where dark energy directly interacts with cold dark matter by exchanging energy and momentum, have attracted significant attention in recent years [42–78] (see Ref. [79] for a recent review). In such interacting dark energy (IDE) scenario, the conservation laws for the energy-momentum tensor ($T_{\mu\nu}$) of dark energy (de) and cold dark matter (c) are modified as

$$\nabla_\nu T_{\mu,de}^\nu = -\nabla_\nu T_{\mu,c}^\nu = Q_\mu, \quad (1)$$

where Q_μ denotes the energy-momentum transfer vector. A specific Q_μ determines the energy transfer rate Q , its perturbation δQ and the momentum transfer rate f . These modifications alter both the background evolution and perturbations of the dark sectors, offering a potential resolution to the coincidence problem [80–83], and introducing new features to the structure formation [84–86].

Actually, the expansion history of the Universe in IDE and dynamical dark energy models can mimic each other by adjusting the model's parameters, which means that in this situation a dark energy model with EoS $w \neq -1$ is observationally degenerate with an IDE model with

* Corresponding author; zhangxin@mail.neu.edu.cn

$w = -1$ but $Q \neq 0$. Given that current cosmological data show a preference for dynamical dark energy, it is natural to explore whether this deviation from Λ CDM could instead be explained by a non-zero dark sector interaction. Indeed, recent studies have explored this possibility. For instance, the authors in Ref. [87] combined DESI DR1 BAO, Planck CMB, and PantheonPlus SNIa to constrain an IDE model with Q proportional to the density of dark energy, finding a non-zero coupling constant exceeding the 95% confidence level (CL). Ref. [5] analyzed four IDE models, using similar cosmological data, reporting a non-zero coupling exceeding the 68% CL for three cases (note that 3σ can be reached in the case of $Q = \beta H_0 \rho_{de}$). In our recent work [6], we further examined whether current data support a sign-changed interaction.

While these studies provide valuable insights, their conclusions remain inherently model-dependent. In this work, we present a model-independent reconstruction of the vacuum energy ($w = -1$) interacting with cold dark matter, following the non-parametric framework of Refs. [88, 89]. By discretizing the coupling function and assuming a Gaussian smoothness prior, we reconstruct the coupling without assuming any specific parameterization. We utilize the most recent cosmological observations, including DESI DR1/DR2 BAO measurements, Planck CMB data, and three distinct SNIa samples. This comprehensive analysis enables us to probe the possible dark sector interaction without theoretical bias. We will show that the dynamical dark energy preference in current data can be equally well explained by IDE scenario.

The structure of this paper is organized as follows. In Sec. II, we briefly introduce the IDE model. In Sec. III, we outline how we implement the non-parametric reconstruction. In Sec. IV, we show the cosmological data used in this work, and report the reconstruction results. The conclusion is given in Sec. V.

II. THE MODEL

The conservation laws in the background level for the densities of dark energy (ρ_{de}) and cold dark matter (ρ_c) satisfy

$$\rho'_{de} + 3\mathcal{H}(1+w)\rho_{de} = aQ, \quad (2)$$

$$\rho'_c + 3\mathcal{H}\rho_c = -aQ, \quad (3)$$

where a is the scale factor of the Universe, $w = p_{de}/\rho_{de}$ is the EoS of dark energy, $\mathcal{H} = a'/a$ is the conformal Hubble parameter, and a prime denotes the derivative with respect to the conformal time. In this paper, we set the EoS of dark energy $w = -1$. Namely, we consider the case of vacuum energy interacting with cold dark matter. We assume the energy transfer rate Q to be of the following form

$$Q = \beta(a)H\rho_{de}, \quad (4)$$

where $\beta(a)$ is the dimensionless coupling parameter (that is evolutionary) and H is the Hubble parameter. The specific form of Q is chosen for mathematical convenience without loss of generality, as any arbitrariness in this choice is fully absorbed into the time-dependent coupling function $\beta(a)$. We have verified that alternative forms (e.g., $Q \propto \rho_c$) yield equivalent reconstruction results. For clarity in subsequent discussion, we refer to this framework as the $\beta(a)$ model (or equivalently, the $\beta(z)$ model when expressed in terms of cosmological redshift).

In this study, we avoid imposing any ad hoc parameterization on the coupling function $\beta(a)$. Instead, we reconstruct it from cosmological data using non-parametric approach. Specifically, we discretize the evolution of β by dividing the scale factor interval $[a_{\min}, 1]$ into N bins, treating β as piecewise constant within each bin, i.e.,

$$\beta(a) = \sum_{i=1}^N \beta_i T_i(a), \quad T_i(a) = \begin{cases} 1, & a_i \leq a < a_{i+1}, \\ 0, & \text{otherwise,} \end{cases} \quad (5)$$

where β_i for $i = 1, 2, \dots, N$ denotes the amplitude of each bin. We set $a_1 = a_{\min}$, $a_{N+1} = 1$ and $\beta(a) = 0$ at $a < a_1$. Then the model's background can be solved, and the energy densities of the dark sectors evolve as

$$\rho_{de} = \rho_{de0} \prod_{k=i+1}^N a_k^{\beta_k - \beta_{k-1}} a^{\beta_i}, \quad (6)$$

and

$$\begin{aligned} \rho_c = & \rho_{de0} a^{-3} \sum_{j=i}^{N-1} \prod_{k=j+1}^N a_k^{\beta_k - \beta_{k-1}} \frac{\beta_j}{\beta_j + 3} (a_{j+1}^{\beta_j + 3} - a_j^{\beta_j + 3}) \\ & + \rho_{de0} a^{-3} \prod_{k=i+1}^N a_k^{\beta_k - \beta_{k-1}} \frac{\beta_i}{\beta_i + 3} (a_i^{\beta_i + 3} - a^{\beta_i + 3}) \\ & + \rho_{c0} a^{-3} + \rho_{de0} a^{-3} \frac{\beta_N}{\beta_N + 3} (1 - a_N^{\beta_N + 3}), \end{aligned} \quad (7)$$

at $a_i \leq a < a_{i+1}$ for $i = 1, 2, \dots, N$. Here we set $\sum_{j=N}^{N-1} = 0$ and $\prod_{k=N+1}^N = 1$ for $i = N$ ($a_N \leq a < 1$).

For the model's perturbation, we assume the energy-momentum transfer Q_μ to be parallel to the four-velocity of dark matter, i.e., $Q_\mu = Q u_{\mu,c}$. In the choice, the momentum transfer rate f vanishes in the dark matter rest frame, and hence the dark matter particles follow geodesics. For dark energy, we handle its perturbation using the extended parameterized post-Friedmann (ePPF) approach [90], which is the PPF framework [91, 92] applied to IDE theory. The ePPF approach can help avoid the possible large-scale instability [67, 93, 94] that may occur in standard linear perturbation theory at specific parameter values. In previous works [90, 95], we established the ePPF approach for different IDE models. More recently, we further developed an ePPF approach for a general parametrization IDE model with five free functions C_1 , C_2 , C_3 , D_1 and D_2 [96]. This model-independent formulation allows different IDE scenarios

to be mapped onto the parametrization by specifying these functions. For our specific $\beta(a)$ model, the corresponding forms of the five functions are $C_1 = D_2 = Q$ and $C_2 = C_3 = D_1 = 0$. Further details on the parametrization and the ePPF implementation can be found in Ref. [96].

III. THE RECONSTRUCTION METHOD

To reconstruct the coupling history, $\beta(a)$, we can constrain the amplitude of each bin, β_i , using the data. However, if the neighboring bins are treated as independent, fitting a large number of uncorrelated bins could result in excessively large uncertainties. To avoid this issue, we adopt the non-parametric approach developed in Refs. [88, 89], in which the variable to be reconstructed is assumed to be a smooth function, and hence its values at neighboring points are not entirely independent. This feature for $\beta(a)$ can be described by a correlation function between its values at a and a' ,

$$\xi(|a - a'|) \equiv \langle [\beta(a) - \beta^{\text{fid}}(a)][\beta(a') - \beta^{\text{fid}}(a')] \rangle, \quad (8)$$

with β^{fid} a reference fiducial model. Here $\beta(a)$ is assumed to be a Gaussian random variable with a covariance matrix among a large number of bins given by

$$C_{ij} = \frac{1}{\Delta^2} \int_{a_i}^{a_i + \Delta} da \int_{a_j}^{a_j + \Delta} da' \xi(|a - a'|), \quad (9)$$

where Δ is the bin width. This covariance matrix defines a Gaussian prior probability distribution for β_i , i.e.,

$$\mathcal{P}_{\text{prior}}(\boldsymbol{\beta}) \propto \exp\left(-\frac{1}{2}(\boldsymbol{\beta} - \boldsymbol{\beta}^{\text{fid}})\mathbf{C}^{-1}(\boldsymbol{\beta} - \boldsymbol{\beta}^{\text{fid}})\right). \quad (10)$$

According to Bayes' theorem, the desired posterior probability is proportional to the likelihood of the data times the prior probability,

$$\mathcal{P}(\boldsymbol{\beta}|\mathbf{D}) \propto \mathcal{P}(\mathbf{D}|\boldsymbol{\beta}) \times \mathcal{P}_{\text{prior}}(\boldsymbol{\beta}), \quad (11)$$

which penalizes those models that are less smooth.

The calculation of the covariance matrix depends on a specific $\xi(|a - a'|)$. Following Ref. [97], we assume the correlation function to have the form proposed by Crittenden, Pogosian and Zhao (CPZ) [88],

$$\xi_{\text{CPZ}}(\delta a) = \frac{\xi(0)}{1 + (\delta a/a_c)^2}, \quad (12)$$

where $\delta a \equiv |a - a'|$, a_c describes the typical smoothing scale, and $\xi(0)$ is the normalization factor determined by the expected variance of the mean of β , i.e., $\sigma_\beta^2 \simeq \pi \xi(0) a_c / (1 - a_{\min})$. One can adjust the prior strength by tuning the values of a_c and σ_β^2 . A weak prior (i.e., small a_c or large σ_β^2) can match the true model on average, but will result in a noisy reconstruction, while a stronger

prior reduces the variance but pulls the reconstructed results towards the peak of the prior. In this paper, we set $a_c = 0.06$ and $\sigma_\beta = 0.04$, representing a moderate prior, which was also adopted in Ref. [98]. To avoid the explicit dependence on the fiducial model, one can marginalize over the value of β^{fid} with several ways [97]. In this paper, we use the ‘floating’ average method [97], which takes the fiducial model to be a local average,

$$\beta_i^{\text{fid}} = \sum_{|a_j - a_i| \leq a_c} \beta_j^{\text{true}} / N_j, \quad (13)$$

where N_j is the number of neighboring bins around the i -th bin within the smoothing scale.

IV. DATA AND RESULTS

In this work, we constrain the amplitudes of 20 bins, i.e., $N = 20$, with the first bin covering the wide range of $a \in [0.0001, 0.286]$, and the last 19 bins uniform in $a \in [0.286, 1]$, corresponding to $z \in [0, 2.5]$. We sample the parameter space using the public package **Cobaya** [99] with the nested sampler **PolyChord** [100, 101]. The obtained samples are analyzed using the public package **Getdist** [102]. The Gaussian prior defined in Eq. (10) is computed as an external prior in **Cobaya**. The theoretical model is solved using the **IDECAMB** code [96], which is an implementation of IDE theory in the public Einstein-Boltzmann solver **CAMB** [103, 104]. To ensure compatibility with the **Cobaya** package, we have rewritten the **IDECAMB** code based on the new version of **CAMB**. To ensure numerical stability in nested sampling, we adopt conservative priors on the cosmological parameters: the physical baryon density $\Omega_b h^2 \in [0.01, 0.05]$, the physical cold dark matter density $\Omega_c h^2 \in [0.02, 0.3]$, the Hubble constant $H_0 \in [40, 100]$, the reionization optical depth $\tau_{\text{reio}} \in [0.01, 0.05]$, the amplitude and spectral index of the primordial scalar spectrum $\ln(10^{10} A_s) \in [2.5, 3.5]$ and $n_s \in [0.85, 1.1]$, and the coupling constants $\beta_i \in [-2, 2]$ for $i = 1, 2, \dots, 20$. We take H_0 as a free parameter instead of the commonly used θ_{MC} , because θ_{MC} is dependent on a standard non-interacting background evolution.

We adopt the following datasets:

- **CMB**: For the CMB data, we use the temperature (TT), polarization (EE), cross (TE), and lensing power spectra measurements. The specific likelihoods are: (i) the **Commander** likelihood using the temperature spectrum at large scales ($2 \leq \ell \leq 30$), from the Planck 2018 [31, 105]; (ii) the **SimAll** likelihood using the spectrum of E-mode polarization at large scales ($2 \leq \ell \leq 30$) from the Planck 2018 [31, 105]; (iii) the high- ℓ **CamSpec** ($\ell \geq 30$) likelihood using dust-cleaned TT, TE, and EE power spectra computed from the Planck 2020 (PR4 / NPIPE) maps [106]; (iv) the CMB lensing likelihood from the NPIPE PR4 Planck [107]. We label the combination of these likelihoods as “CMB”.

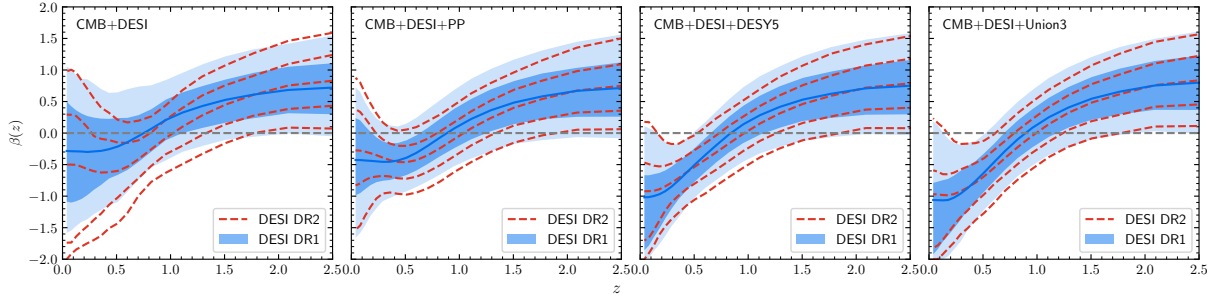


FIG. 1. Reconstructed evolution history of $\beta(z)$ with the mean value and 68% and 95% CL errors for the baseline CMB+DESI and its individual combinations with each SNIa dataset (PP, DESY5, and Union3). The blue solid lines and filled regions represent the DESI DR1-based reconstructions, while the red dashed lines show the DR2-based results. The black dashed lines denote the Λ CDM prediction ($\beta = 0$).

- BAO: We utilize the BAO measurements from the DESI DR2 [4], which includes tracers from the bright galaxy sample (BGS), luminous red galaxies (LRG), emission line galaxies (ELG), quasars (QSO), and the Ly α forest in a redshift range $0.1 \leq z \leq 4.2$. These tracers are described through the transverse comoving distance D_M/r_d , the angle-averaged distance D_V/r_d , and the Hubble horizon D_H/r_d , where r_d is the comoving sound horizon at the drag epoch. We also compare with the results from DR1 [3].

- SNIa: We adopt SNIa data from three compilations: (i) the PantheonPlus (PP) dataset, which comprises 1550 spectroscopically confirmed SNIa in the redshift range of $0.001 < z < 2.26$ [108] (The public likelihood imposes a bound of $z > 0.01$ in order to mitigate the impact of peculiar velocities in the Hubble diagram); (ii) the Dark Energy Survey Year 5 (DESY5) data release, which includes 194 low-redshift SNIa ($0.025 < z < 0.1$) and 1635 SNIa classified photometrically, covering the range $0.1 < z < 1.3$ [109]; (iii) the more recent Union3 compilation, presented in Ref. [110], including 2087 SNIa, with many (1363 SNIa) overlapping with those in Pantheon-Plus. These SNIa datasets are not independent of each other. Therefore, we do not combine them but instead present results from CMB+DESI plus each SNIa dataset independently.

Convergence in PolyChord is achieved when the fraction of the total evidence contained in the live points falls below 0.001. In Fig. 1, we plot the reconstructed $\beta(z)$ with the mean value and 68% and 95% CL errors for the baseline CMB+DESI and its individual combinations with each SNIa dataset (PP, DESY5, and Union3). The blue solid lines and filled regions represent the DESI DR1-based reconstructions, while the red dashed lines show the DR2-based results. A key feature across all reconstructions is that the mean value of $\beta(z)$ changes sign during its evolution. Specifically, it is positive at early times, suggesting an energy transfer from cold dark matter to dark energy, but turns negative at late times, implying an energy flow in the reverse direction. This behavior is consistent with the findings of Ref. [6], in which

TABLE I. Summary of the $\Delta\chi_{\text{MAP}}^2$ values, the difference of χ^2 in the maximum a posteriori (MAP) between the $\beta(z)$ model and the Λ CDM model, for the different combinations of datasets as indicated. The third column lists the corresponding Bayes factor in logarithmic space, $\ln \mathcal{B} = \ln Z_{\beta(z)} - \ln Z_{\Lambda\text{CDM}}$, where $\ln Z_{\beta(z)}$ and $\ln Z_{\Lambda\text{CDM}}$ represent the Bayesian evidence of the $\beta(z)$ model and Λ CDM, respectively.

Datasets	$\Delta\chi_{\text{MAP}}^2$	$\ln \mathcal{B}$
CMB+DESI DR1	-5.46	1.36 ± 0.68
CMB+DESI DR2	-4.37	1.44 ± 0.70
CMB+DESI DR1+PP	-5.49	-0.19 ± 0.64
CMB+DESI DR2+PP	-7.88	1.12 ± 0.69
CMB+DESI DR1+DESY5	-13.45	3.42 ± 0.68
CMB+DESI DR2+DESY5	-17.76	5.98 ± 0.69
CMB+DESI DR1+Union3	-10.94	1.92 ± 0.70
CMB+DESI DR2+Union3	-9.78	3.57 ± 0.69

the coupling is reconstructed with a parametric model.

When reconstruction uncertainties are taken into account, all data combinations yield a positive $\beta(z)$ that deviates from the Λ CDM prediction ($\beta = 0$) at approximately 2σ at high redshifts. At low redshifts, however, the results vary depending on whether and which SNIa dataset is used. The CMB+DESI and the CMB+DESI+PP data get a $\beta(z)$ consistent with a zero coupling within 2σ , whereas CMB+DESI+DESY5 and CMB+DESI+Union3 show a preference for negative β at about 2σ level. The DESI DR2-based results are consistent with those from DR1, but show lower reconstruction uncertainties in the redshift range $0.3 < z < 2.5$. This improvement aligns with the primary redshift coverage of DESI observations and reflects the enhanced precision achieved in DR2.

To assess the improvements in goodness of fit, we compute $\Delta\chi_{\text{MAP}}^2$, the difference of χ^2 in the maximum a posteriori (MAP) between the $\beta(z)$ model and the Λ CDM

model, using the minimizer sampler [111–113] in Cobaya. In Table I, we summarize the $\Delta\chi^2_{\text{MAP}}$ values for the different data combinations. Across all dataset combinations, the $\beta(z)$ model yields a better fit than ΛCDM , with the most notable improvement occurring for CMB+DESI DR2+DESY5. For the baseline CMB + DESI analysis, we observe $\Delta\chi^2_{\text{MAP}} = -5.46$ (DR1) and -4.37 (DR2). The inclusion of SNIa data consistently enhances the preference for the $\beta(z)$ model over ΛCDM , though the degree of improvement varies across datasets. For the CMB + DESI + PP data combination, we find moderate improvements in fit quality, with $\Delta\chi^2_{\text{MAP}} = -5.49$ for DR1 and -7.88 for DR2. In contrast, DESY5 demonstrates the most pronounced preference, yielding $\Delta\chi^2_{\text{MAP}} = -13.45$ (DR1) and -17.76 (DR2). Similarly, Union3 shows strong but slightly weaker improvements, with $\Delta\chi^2_{\text{MAP}} = -10.94$ (DR1) and -9.78 (DR2).

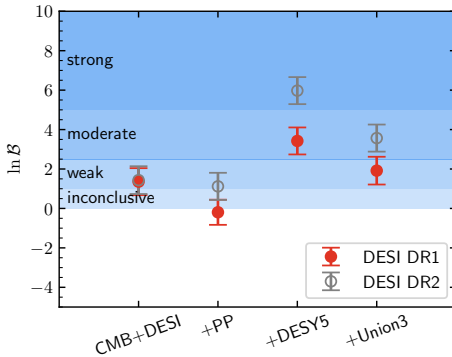


FIG. 2. The Bayes factor $\ln \mathcal{B}$ results with 68% CL errors for different data combinations. The shaded regions correspond to the Jeffreys' scale thresholds for evidence interpretation: $|\ln \mathcal{B}| < 1$ (inconclusive), $1 \leq |\ln \mathcal{B}| < 2.5$ (weak), $2.5 \leq |\ln \mathcal{B}| < 5$ (moderate), and $|\ln \mathcal{B}| \geq 5$ (strong).

However, the χ^2 test does not account for model complexity or the number of parameters involved. To address this limitation, we further compute the Bayes factor in logarithmic space, $\ln \mathcal{B} = \ln Z_{\beta(z)} - \ln Z_{\Lambda\text{CDM}}$, where $\ln Z_{\beta(z)}$ and $\ln Z_{\Lambda\text{CDM}}$ represent the Bayesian evidence of the $\beta(z)$ model and ΛCDM , respectively. The Bayesian evidence is directly obtained from the PolyChord sampler output, though we note that the external prior defined in Eq. (10) is unnormalized by default. Thus, the raw evidence Z_u must be corrected by the prior volume Z_π as $\ln Z_{\beta(z)} = \ln Z_u - \ln Z_\pi$. The $\ln \mathcal{B}$ results with 68% CL errors are summarized in Table I and shown in Fig. 2. For visual reference, Fig. 2 includes shaded regions corresponding to the Jeffreys' scale thresholds [114, 115] for evidence interpretation. Our analysis demonstrates a consistent trend of stronger evidence for the $\beta(z)$ model in DESI DR2 compared to DR1 across all data combinations. For CMB + DESI DR1/DR2, we find $\ln \mathcal{B} = 1.36 \pm 0.68/1.44 \pm 0.70$, indicating *weak evidence* in both cases, with DR2 showing slightly stronger (but statistically consistent) preference.

The inclusion of PP SNIa yields $\ln \mathcal{B} = -0.19 \pm 0.64$ (DR1) and 1.12 ± 0.69 (DR2) – while DR1 remains *inconclusive*, DR2 crosses the threshold into *weak evidence* territory. Most significantly, CMB + DESI + DESY5 shows $\ln \mathcal{B} = 3.42 \pm 0.68$ (DR1) and 5.98 ± 0.69 (DR2). Here, DR1 provides *moderate evidence* while DR2 reaches *strong evidence*. Similarly, CMB + DESI + Union3 transitions from *moderate* (1.92 ± 0.70) to *strong* (3.57 ± 0.69) evidence from DR1 to DR2.

The positive values of $\ln \mathcal{B}$ imply that the improved goodness of fit in the $\beta(z)$ model outweighs the Occam's razor penalty arising from parameter space integration. This implies that only a subset of the additional parameters is effectively constrained by the data. To quantify this, we assess the number of effective degrees of freedom introduced by the $\beta(z)$ model relative to ΛCDM . We perform a principal component analysis (PCA) on the posterior distribution by diagonalizing the covariance matrix of the β bins after marginalizing over other cosmological parameters. The eigenvectors $e_i(z)$ form a basis for expanding $\beta(z)$ as $\beta(z) = \sum_{i=1}^N \alpha_i e_i(z)$, while the eigenvalues λ_i determine the measurement precision of each mode, with $\sigma(\alpha_i) = \sqrt{\lambda_i}$ [116].

As a representative example, Fig. 3 displays the inverse eigenvalues of the posterior covariance matrices for the four DESI DR1-based data combinations, ordered by the number of nodes in the eigenvectors $e_i(z)$. For comparison, we also plot the inverse eigenvalues derived from the prior-only covariance matrix. The results reveal a clear distinction: while the first three posterior inverse eigenvalues significantly exceed their prior counterparts, the fourth and higher eigenvalues show close agreement with the prior values. This demonstrates that only the first three principal components are data-constrained, whereas the higher-order modes remain prior-dominated. We therefore conclude that the $\beta(z)$ model effectively introduces three additional degrees of freedom compared to ΛCDM . These three data-dominated eigenvectors $e_i(z)$ are presented in Fig. 4. By projecting the mean $\beta(z)$ onto these three data-dominated eigenvectors, i.e., $\beta(z) = \sum_{i=1}^3 \alpha_i e_i(z)$, we derive the constraints on the coefficients α_i (mean values and 68% CL errors), as summarized in Table II. The improvement in fit $\Delta\chi^2_{\text{MAP}}$ is well approximated by $\sum_{i=1}^3 [\alpha_i/\sigma(\alpha_i)]^2$, confirming that these three principal components account for nearly all the enhanced model performance.

TABLE II. The coefficients α_i (mean values and 68% CL errors) of the first three data-dominated modes for the four DESI DR1-based data combinations.

	CMB+DESI	+PP	+DESY5	+Union3
α_1	-1.16 ± 0.68	-0.35 ± 0.37	-0.65 ± 0.36	0.44 ± 0.50
α_2	-1.05 ± 1.62	-1.08 ± 1.16	-2.67 ± 1.18	-2.99 ± 1.25
α_3	0.92 ± 0.97	1.80 ± 0.87	1.42 ± 0.85	1.53 ± 0.86

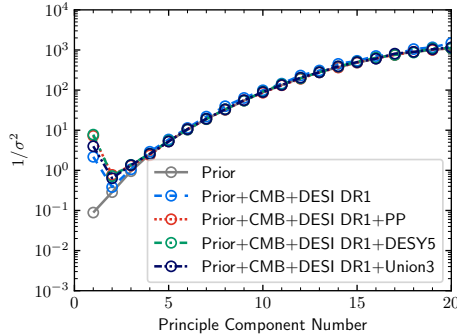


FIG. 3. The inverse eigenvalues of both the prior and the four posterior covariance matrices, ordered by the number of nodes in $e_i(z)$.

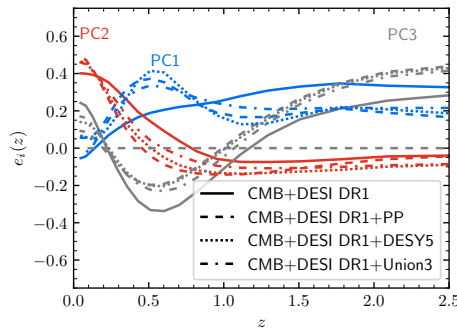


FIG. 4. The first three data-dominated eigenvectors $e_i(z)$ for the four DESI DR1-based data combinations.

V. CONCLUSION

In this study, we conduct a model-independent reconstruction of the vacuum energy ($w = -1$) interacting with cold dark matter, using the latest cosmological data, including DESI DR1/DR2 BAO measurements, Planck CMB data, and three distinct SNIa datasets (PP, DESY5, and Union3). By employing a non-parametric approach with a Gaussian smoothness prior, we reconstruct the coupling function $\beta(z)$ without assuming any specific parameterization. The results consistently show a sign change in the mean value of $\beta(z)$ during cosmic evolution, transitioning from positive values at early times (indicating energy transfer from dark matter to

dark energy) to negative values at late times (suggesting a reversed energy flow). When considering reconstruction uncertainties, all data combinations yield a positive β that deviates from the Λ CDM prediction ($\beta = 0$) at approximately 2σ at high redshifts. At low redshifts, the CMB+DESI and the CMB+DESI+PP data get a β consistent with a zero coupling within 2σ , whereas CMB+DESI+DESY5 and CMB+DESI+Union3 show a preference for negative β at about 2σ level. The DESI DR2-based results are consistent with those from DR1, but show slightly reduced uncertainties. The $\beta(z)$ model provides a better fit to the data compared to Λ CDM, as evidenced by improvements in $\Delta\chi^2_{\text{MAP}}$ and Bayesian evidence ($\ln \mathcal{B}$). Notably, the CMB+DESI DR2+DESY5 data yield the strongest evidence for the sign-reversal IDE scenario, reaching the “strong” threshold on the Jeffreys’ scale. Principal component analysis reveals that the data effectively constrain three additional degrees of freedom in the $\beta(z)$ model, accounting for most of the improvement in goodness of fit.

While current observations show intriguing hints of dynamical dark energy, our analysis demonstrates that these signatures could equally originate from dark sector interactions. This degeneracy presents a fundamental challenge in understanding the true nature of cosmic acceleration. The IDE model cannot be distinguished from the uncoupled dark energy model in the background evolution since the expansion history of the Universe given by the two can mimic each other by adjusting the values of their parameters. Fortunately, the dynamics of dark matter can be altered by dark energy in an IDE model, leading to modified structure growth that distinguishes these scenarios from uncoupled dark energy models. We expect that future observations incorporating structure formation information could help break this degeneracy.

ACKNOWLEDGMENTS

We thank Tian-Nuo Li and Guo-Hong Du for their helpful discussions. This work was supported by the National SKA Program of China (Grants Nos. 2022SKA0110200 and 2022SKA0110203), the National Natural Science Foundation of China (Grants Nos. 12473001, 11975072, 11835009, and 11805031), and the China Manned Space Program (Grant No. CMS-CSST-2025-A02).

-
- [1] A. G. Adame *et al.* (DESI), *JCAP* **04**, 012 (2025), [arXiv:2404.03000 \[astro-ph.CO\]](#).
 - [2] A. G. Adame *et al.* (DESI), *JCAP* **01**, 124 (2025), [arXiv:2404.03001 \[astro-ph.CO\]](#).
 - [3] A. G. Adame *et al.* (DESI), *JCAP* **02**, 021 (2025), [arXiv:2404.03002 \[astro-ph.CO\]](#).
 - [4] M. Abdul Karim *et al.* (DESI), (2025), [arXiv:2503.14738 \[astro-ph.CO\]](#).
 - [5] T.-N. Li, P.-J. Wu, G.-H. Du, S.-J. Jin, H.-L. Li, J.-F. Zhang, and X. Zhang, *Astrophys. J.* **976**, 1 (2024), [arXiv:2407.14934 \[astro-ph.CO\]](#).
 - [6] T.-N. Li, G.-H. Du, Y.-H. Li, P.-J. Wu, S.-J. Jin, J.-F. Zhang, and X. Zhang, (2025), [arXiv:2501.07361 \[astro-ph.CO\]](#).
 - [7] T.-N. Li, Y.-H. Li, G.-H. Du, P.-J. Wu, L. Feng, J.-F. Zhang, and X. Zhang, *Eur. Phys. J. C* **85**, 608 (2025),

- arXiv:2411.08639 [astro-ph.CO].
- [8] T.-N. Li, Y.-M. Zhang, Y.-H. Yao, P.-J. Wu, J.-F. Zhang, and X. Zhang, (2025), arXiv:2506.09819 [astro-ph.CO].
- [9] G.-H. Du, P.-J. Wu, T.-N. Li, and X. Zhang, *Eur. Phys. J. C* **85**, 392 (2025), arXiv:2407.15640 [astro-ph.CO].
- [10] G.-H. Du, T.-N. Li, P.-J. Wu, L. Feng, S.-H. Zhou, J.-F. Zhang, and X. Zhang, (2025), arXiv:2501.10785 [astro-ph.CO].
- [11] P.-J. Wu and X. Zhang, (2024), arXiv:2411.06356 [astro-ph.CO].
- [12] J.-L. Ling, G.-H. Du, T.-N. Li, J.-F. Zhang, S.-J. Wang, and X. Zhang, (2025), arXiv:2505.22369 [astro-ph.CO].
- [13] Y. Yang, X. Ren, Q. Wang, Z. Lu, D. Zhang, Y.-F. Cai, and E. N. Saridakis, *Sci. Bull.* **69**, 2698 (2024), arXiv:2404.19437 [astro-ph.CO].
- [14] Y. Yang, Q. Wang, X. Ren, E. N. Saridakis, and Y.-F. Cai, (2025), arXiv:2504.06784 [astro-ph.CO].
- [15] C. Li, J. Wang, D. Zhang, E. N. Saridakis, and Y.-F. Cai, (2025), arXiv:2504.07791 [astro-ph.CO].
- [16] Y. Cai, X. Ren, T. Qiu, M. Li, and X. Zhang, (2025), arXiv:2505.24732 [astro-ph.CO].
- [17] G. Ye, M. Martinelli, B. Hu, and A. Silvestri, *Phys. Rev. Lett.* **134**, 181002 (2025), arXiv:2407.15832 [astro-ph.CO].
- [18] Z. Wang, S. Lin, Z. Ding, and B. Hu, *Mon. Not. Roy. Astron. Soc.* **534**, 3869 (2024), arXiv:2405.02168 [astro-ph.CO].
- [19] Y.-H. Pang, X. Zhang, and Q.-G. Huang, *JCAP* **04**, 057 (2025), arXiv:2411.14189 [astro-ph.CO].
- [20] Y.-H. Pang, X. Zhang, and Q.-G. Huang, (2025), arXiv:2503.21600 [astro-ph.CO].
- [21] Y.-H. Pang, X. Zhang, and Q.-G. Huang, *Phys. Rev. D* **111**, 123504 (2025), arXiv:2408.14787 [astro-ph.CO].
- [22] L. Huang, R.-G. Cai, and S.-J. Wang, (2025), arXiv:2502.04212 [astro-ph.CO].
- [23] H. Wang and Y.-S. Piao, (2024), arXiv:2404.18579 [astro-ph.CO].
- [24] H. Wang, Z.-Y. Peng, and Y.-S. Piao, *Phys. Rev. D* **111**, L061306 (2025), arXiv:2406.03395 [astro-ph.CO].
- [25] W. Giarè, M. Najafi, S. Pan, E. Di Valentino, and J. T. Firouzjaee, *JCAP* **10**, 035 (2024), arXiv:2407.16689 [astro-ph.CO].
- [26] J.-Q. Jiang, W. Giarè, S. Gariazzo, M. G. Dainotti, E. Di Valentino, O. Mena, D. Pedrotti, S. S. da Costa, and S. Vagnozzi, *JCAP* **01**, 153 (2025), arXiv:2407.18047 [astro-ph.CO].
- [27] M. Abedin, L. A. Escamilla, S. Pan, E. Di Valentino, and W. Yang, (2025), arXiv:2505.09470 [astro-ph.CO].
- [28] J.-Q. Jiang, D. Pedrotti, S. S. da Costa, and S. Vagnozzi, *Phys. Rev. D* **110**, 123519 (2024), arXiv:2408.02365 [astro-ph.CO].
- [29] D. Wang, (2024), arXiv:2404.06796 [astro-ph.CO].
- [30] A. G. Riess, W.-L. Yuan, L. M. Macri, *et al.*, *Astrophys. J. Lett.* **934**, L7 (2022), arXiv:2112.04510 [astro-ph.CO].
- [31] N. Aghanim, Y. Akrami, M. Ashdown, *et al.* (Planck), *Astron. Astrophys.* **641**, A6 (2020), [Erratum: *Astron. Astrophys.* 652, C4 (2021)], arXiv:1807.06209 [astro-ph.CO].
- [32] S. Weinberg, *Rev. Mod. Phys.* **61**, 1 (1989).
- [33] V. Sahni and A. A. Starobinsky, *Int. J. Mod. Phys. D* **9**, 373 (2000), arXiv:astro-ph/9904398.
- [34] P. J. E. Peebles and B. Ratra, *Rev. Mod. Phys.* **75**, 559 (2003), arXiv:astro-ph/0207347.
- [35] R. Bean, S. M. Carroll, and M. Trodden, (2005), arXiv:astro-ph/0510059.
- [36] E. J. Copeland, M. Sami, and S. Tsujikawa, *Int. J. Mod. Phys. D* **15**, 1753 (2006), arXiv:hep-th/0603057.
- [37] V. Sahni and A. Starobinsky, *Int. J. Mod. Phys. D* **15**, 2105 (2006), arXiv:astro-ph/0610026.
- [38] M. Kamionkowski (2007) arXiv:0706.2986 [astro-ph].
- [39] J. Frieman, M. Turner, and D. Huterer, *Ann. Rev. Astron. Astrophys.* **46**, 385 (2008), arXiv:0803.0982 [astro-ph].
- [40] M. Li, X.-D. Li, S. Wang, and Y. Wang, *Commun. Theor. Phys.* **56**, 525 (2011), arXiv:1103.5870 [astro-ph.CO].
- [41] D. H. Weinberg, M. J. Mortonson, D. J. Eisenstein, C. Hirata, A. G. Riess, and E. Rozo, *Phys. Rept.* **530**, 87 (2013), arXiv:1201.2434 [astro-ph.CO].
- [42] J.-H. He and B. Wang, *JCAP* **06**, 010 (2008), arXiv:0801.4233 [astro-ph].
- [43] J.-H. He, B. Wang, and Y. P. Jing, *JCAP* **07**, 030 (2009), arXiv:0902.0660 [gr-qc].
- [44] J.-H. He, B. Wang, and P. Zhang, *Phys. Rev. D* **80**, 063530 (2009), arXiv:0906.0677 [gr-qc].
- [45] Z.-K. Guo, R.-G. Cai, and Y.-Z. Zhang, *JCAP* **05**, 002 (2005), arXiv:astro-ph/0412624.
- [46] H. Wei and R.-G. Cai, *Eur. Phys. J. C* **59**, 99 (2009), arXiv:0707.4052 [hep-th].
- [47] R.-G. Cai and Q. Su, *Phys. Rev. D* **81**, 103514 (2010), arXiv:0912.1943 [astro-ph.CO].
- [48] J.-H. He, B. Wang, and E. Abdalla, *Phys. Rev. D* **83**, 063515 (2011), arXiv:1012.3904 [astro-ph.CO].
- [49] C. G. Boehmer, G. Caldera-Cabral, R. Lazkoz, and R. Maartens, *Phys. Rev. D* **78**, 023505 (2008), arXiv:0801.1565 [gr-qc].
- [50] Z.-K. Guo, N. Ohta, and S. Tsujikawa, *Phys. Rev. D* **76**, 023508 (2007), arXiv:astro-ph/0702015.
- [51] J.-Q. Xia, *Phys. Rev. D* **80**, 103514 (2009), arXiv:0911.4820 [astro-ph.CO].
- [52] H. Wei, *Commun. Theor. Phys.* **56**, 972 (2011), arXiv:1010.1074 [gr-qc].
- [53] Y.-H. Li and X. Zhang, *Eur. Phys. J. C* **71**, 1700 (2011), arXiv:1103.3185 [astro-ph.CO].
- [54] X. Zhang, F.-Q. Wu, and J. Zhang, *JCAP* **01**, 003 (2006), arXiv:astro-ph/0411221.
- [55] Y.-H. Li and X. Zhang, *Phys. Rev. D* **89**, 083009 (2014), arXiv:1312.6328 [astro-ph.CO].
- [56] Y. Wang, D. Wands, L. Xu, J. De-Santiago, and A. Hojjati, *Phys. Rev. D* **87**, 083503 (2013), arXiv:1301.5315 [astro-ph.CO].
- [57] A. Poutsidou, C. Skordis, and E. J. Copeland, *Phys. Rev. D* **88**, 083505 (2013), arXiv:1307.0458 [astro-ph.CO].
- [58] T. Yang, Z.-K. Guo, and R.-G. Cai, *Phys. Rev. D* **91**, 123533 (2015), arXiv:1505.04443 [astro-ph.CO].
- [59] W. Yang, S. Pan, and D. F. Mota, *Phys. Rev. D* **96**, 123508 (2017), arXiv:1709.00006 [astro-ph.CO].
- [60] R.-G. Cai, N. Tamanini, and T. Yang, *JCAP* **05**, 031 (2017), arXiv:1703.07323 [astro-ph.CO].
- [61] W. Yang, S. Pan, E. Di Valentino, R. C. Nunes, S. Vagnozzi, and D. F. Mota, *JCAP* **09**, 019 (2018), arXiv:1805.08252 [astro-ph.CO].
- [62] R. Kase and S. Tsujikawa, *JCAP* **11**, 032 (2020), arXiv:2005.13809 [gr-qc].
- [63] M. S. Linton, R. Crittenden, and A. Poutsidou, *JCAP*

- [68]** Y.-F. Cai, A. Marciano, D.-G. Wang, and E. Wilson-Ewing, *Universe* **3**, 1 (2016), arXiv:1610.00938 [astro-ph.CO].
- [69]** M. Abedin, G.-J. Wang, Y.-Z. Ma, and S. Pan, (2025), arXiv:2505.04336 [astro-ph.CO].
- [70]** L. A. Escamilla, O. Akarsu, E. Di Valentino, and J. A. Vazquez, *JCAP* **11**, 051 (2023), arXiv:2305.16290 [astro-ph.CO].
- [71]** S. Pan, S. Paul, E. N. Saridakis, and W. Yang, (2025), arXiv:2504.00994 [astro-ph.CO].
- [72]** A. Aboubrahim and P. Nath, (2024), arXiv:2411.11177 [astro-ph.CO].
- [73]** E. Di Valentino, O. Mena, S. Pan, L. Visinelli, W. Yang, A. Melchiorri, D. F. Mota, A. G. Riess, and J. Silk, *Class. Quant. Grav.* **38**, 153001 (2021), arXiv:2103.01183 [astro-ph.CO].
- [74]** E. Di Valentino, A. Melchiorri, O. Mena, S. Pan, and W. Yang, *Mon. Not. Roy. Astron. Soc.* **502**, L23 (2021), arXiv:2011.00283 [astro-ph.CO].
- [75]** E. Silva, M. A. Sabogal, M. Scherer, R. C. Nunes, E. Di Valentino, and S. Kumar, *Phys. Rev. D* **111**, 123511 (2025), arXiv:2503.23225 [astro-ph.CO].
- [76]** M. Forconi, W. Giarè, O. Mena, Ruchika, E. Di Valentino, A. Melchiorri, and R. C. Nunes, *JCAP* **05**, 097 (2024), arXiv:2312.11074 [astro-ph.CO].
- [77]** R. C. Nunes, S. Vagnozzi, S. Kumar, E. Di Valentino, and O. Mena, *Phys. Rev. D* **105**, 123506 (2022), arXiv:2203.08093 [astro-ph.CO].
- [78]** B. Wang, E. Abdalla, F. Atrio-Barandela, and D. Pavón, *Rept. Prog. Phys.* **79**, 096901 (2016), arXiv:1603.08299 [astro-ph.CO].
- [79]** B. Wang, E. Abdalla, F. Atrio-Barandela, and D. Pavón, *Rept. Prog. Phys.* **87**, 036901 (2024), arXiv:2402.00819 [astro-ph.CO].
- [80]** L. Amendola, *Phys. Rev. D* **62**, 043511 (2000), arXiv:astro-ph/9908023.
- [81]** D. Comelli, M. Pietroni, and A. Riotto, *Phys. Lett. B* **571**, 115 (2003), arXiv:hep-ph/0302080.
- [82]** X. Zhang, *Mod. Phys. Lett. A* **20**, 2575 (2005), arXiv:astro-ph/0503072.
- [83]** R.-G. Cai and A. Wang, *JCAP* **03**, 002 (2005), arXiv:hep-th/0411025.
- [84]** L. Amendola and D. Tocchini-Valentini, *Phys. Rev. D* **66**, 043528 (2002), arXiv:astro-ph/0111535.
- [85]** O. Bertolami, F. Gil Pedro, and M. Le Delliou, *Phys. Lett. B* **654**, 165 (2007), arXiv:astro-ph/0703462.
- [86]** K. Koyama, R. Maartens, and Y.-S. Song, *JCAP* **10**, 017 (2009), arXiv:0907.2126 [astro-ph.CO].
- [87]** W. Giarè, M. A. Sabogal, R. C. Nunes, and E. Di Valentino, *Phys. Rev. Lett.* **133**, 251003 (2024), arXiv:2404.15232 [astro-ph.CO].
- [88]** R. G. Crittenden, L. Pogosian, and G.-B. Zhao, *JCAP* **12**, 025 (2009), arXiv:astro-ph/0510293.
- [89]** G.-B. Zhao, R. G. Crittenden, L. Pogosian, and X. Zhang, *Phys. Rev. Lett.* **109**, 171301 (2012), arXiv:1207.3804 [astro-ph.CO].
- [90]** Y.-H. Li, J.-F. Zhang, and X. Zhang, *Phys. Rev. D* **90**, 063005 (2014), arXiv:1404.5220 [astro-ph.CO].
- [91]** W. Hu, *Phys. Rev. D* **77**, 103524 (2008), arXiv:0801.2433 [astro-ph].
- [92]** W. Fang, W. Hu, and A. Lewis, *Phys. Rev. D* **78**, 087303 (2008), arXiv:0808.3125 [astro-ph].
- [93]** J.-H. He, B. Wang, and E. Abdalla, *Phys. Lett. B* **671**, 139 (2009), arXiv:0807.3471 [gr-qc].
- [94]** T. Clemson, K. Koyama, G.-B. Zhao, R. Maartens, and J. Valiviita, *Phys. Rev. D* **85**, 043007 (2012), arXiv:1109.6234 [astro-ph.CO].
- [95]** Y.-H. Li, J.-F. Zhang, and X. Zhang, *Phys. Rev. D* **90**, 123007 (2014), arXiv:1409.7205 [astro-ph.CO].
- [96]** Y.-H. Li and X. Zhang, *JCAP* **09**, 046 (2023), arXiv:2306.01593 [astro-ph.CO].
- [97]** R. G. Crittenden, G.-B. Zhao, L. Pogosian, L. Samushia, and X. Zhang, *JCAP* **02**, 048 (2012), arXiv:1112.1693 [astro-ph.CO].
- [98]** Y. Wang, G.-B. Zhao, D. Wands, L. Pogosian, and R. G. Crittenden, *Phys. Rev. D* **92**, 103005 (2015), arXiv:1505.01373 [astro-ph.CO].
- [99]** J. Torrado and A. Lewis, *JCAP* **05**, 057 (2021), arXiv:2005.05290 [astro-ph.IM].
- [100]** W. J. Handley, M. P. Hobson, and A. N. Lasenby, *Mon. Not. Roy. Astron. Soc.* **450**, L61 (2015), arXiv:1502.01856 [astro-ph.CO].
- [101]** W. J. Handley, M. P. Hobson, and A. N. Lasenby, *Mon. Not. Roy. Astron. Soc.* **453**, 4385 (2015), arXiv:1506.00171 [astro-ph.IM].
- [102]** A. Lewis, (2019), arXiv:1910.13970 [astro-ph.IM].
- [103]** A. Lewis, A. Challinor, and A. Lasenby, *Astrophys. J.* **538**, 473 (2000), arXiv:astro-ph/9911177.
- [104]** C. Howlett, A. Lewis, A. Hall, and A. Challinor, *JCAP* **04**, 027 (2012), arXiv:1201.3654 [astro-ph.CO].
- [105]** N. Aghanim *et al.* (Planck), *Astron. Astrophys.* **641**, A5 (2020), arXiv:1907.12875 [astro-ph.CO].
- [106]** E. Rosenberg, S. Gratton, and G. Efstathiou, *Mon. Not. Roy. Astron. Soc.* **517**, 4620 (2022), arXiv:2205.10869 [astro-ph.CO].
- [107]** J. Carron, M. Mirmelstein, and A. Lewis, *JCAP* **09**, 039 (2022), arXiv:2206.07773 [astro-ph.CO].
- [108]** D. Brout *et al.*, *Astrophys. J.* **938**, 110 (2022), arXiv:2202.04077 [astro-ph.CO].
- [109]** T. M. C. Abbott, M. Acevedo, M. Aguena, *et al.* (DES), (2024), arXiv:2401.02929 [astro-ph.CO].
- [110]** D. Rubin *et al.*, (2023), arXiv:2311.12098 [astro-ph.CO].
- [111]** M. J. D. Powell, Technical Report, Department of Applied Mathematics and Theoretical Physics (2009).
- [112]** C. Cartis, J. Fiala, B. Marteau, and L. Roberts, (2018), arXiv:1804.00154 [math.OC].
- [113]** C. Cartis, L. Roberts, and O. Sheridan-Methven, *Optimization* **71**, 2343 (2021), arXiv:1812.11343 [math.OC].
- [114]** R. E. Kass and A. E. Raftery, *J. Am. Statist. Assoc.* **90**, 773 (1995).
- [115]** R. Trotta, *Contemp. Phys.* **49**, 71 (2008), arXiv:0803.4089 [astro-ph].
- [116]** D. Huterer and G. Starkman, *Phys. Rev. Lett.* **90**, 031301 (2003), arXiv:astro-ph/0207517.